Quantum molecular dynamics study on the proton exchange, ionic structures, and transport properties of warm dense hydrogen-deuterium mixtures

Lei Liu,[1,2] Zhi-Guo Li,[2] Jia-Yu Dai,[3] Qi-Feng Chen,[2,*] and Xiang-Rong Chen[1,†]

[1]*Institute of Atomic and Molecular Physics, College of Physical Science and Technology, Sichuan University, Chengdu 610064, People's Republic of China*

[2]*National Key Laboratory for Shock Wave and Detonation Physics Research, Institute of Fluid Physics, China Academy of Engineering Physics, Mianyang 621900, People's Republic of China*

[3]*Department of Physics, National University of Defense Technology, Changsha 410073, People's Republic of China*

(Received 23 February 2018; published 12 June 2018)

Comprehensive knowledge of physical properties such as equation of state (EOS), proton exchange, dynamic structures, diffusion coefficients, and viscosities of hydrogen-deuterium mixtures with densities from 0.1 to 5 g/cm^3 and temperatures from 1 to 50 kK has been presented via quantum molecular dynamics (QMD) simulations. The existing multi-shock experimental EOS provides an important benchmark to evaluate exchange-correlation functionals. The comparison of simulations with experiments indicates that a nonlocal van der Waals density functional (vdW-DF1) produces excellent results. Fraction analysis of molecules using a weighted integral over pair distribution functions was performed. A dissociation diagram together with a boundary where the proton exchange ($H_2 + D_2 \rightleftharpoons 2HD$) occurs was generated, which shows evidence that the HD molecules form as the H_2 and D_2 molecules are almost 50% dissociated. The mechanism of proton exchange can be interpreted as a process of dissociation followed by recombination. The ionic structures at extreme conditions were analyzed by the effective coordination number model. High-order cluster, circle, and chain structures can be founded in the strongly coupled warm dense regime. The present QMD diffusion coefficient and viscosity can be used to benchmark two analytical one-component plasma (OCP) models: the Coulomb and Yukawa OCP models.

DOI: 10.1103/PhysRevE.97.063204

I. INTRODUCTION

Warm dense matter (WDM) has been an ongoing topic in the scientific community over the past decades, linking the traditional definition of condensed matter physics and hot dense matter [1,2]. Warm dense hydrogen and its isotopes play a critical role in understanding the material behaviors under extreme conditions and have a broad application in energy sources [3] as well as astrophysics [4,5]. The equation of state (EOS) and transport properties of them are input parameters for radiation-hydrodynamics simulations which are essential to understand and design the inertial confined fusion (ICF) experiment [3,6–8]. And these parameters will also help to understand the interior structures and evolution of giant planets [9–11]. Consequently, experiments using different loading techniques including gas-gun [12,13], magnetically driven [14–16], laser driven [17–19], and explosive driven [20] have been applied to obtain the EOS of hydrogen and deuterium. Various theoretical methods such as chemical models [21–23] and *ab initio* methods [24,25] were carried out to study the properties of hydrogen and its isotopes.

Compared with the pure systems, mixtures, in general, have a much richer phase diagram than their pure constituents and various effects can be observed only in these multi-component systems [26–28]. The research of mixtures is one of the topics that can count on a great deal of interest from both experimental and theoretical physicists nowadays. Not only the widespread abundance of mixtures in our daily life and in our universe but also the surprising new phenomena which were detected in the laboratories are responsible for this increasing attention. Specially, we concentrate on a mixture of H_2 and D_2 due to the fact that it is a desirable surrogate material for simulating and understanding the characteristics of ICF implosion by considering isotopic effect. Several experiments [29–31] showed that a process of proton exchange takes place to form HD diatomic molecule when an H-D mixture is compressed to high pressures at room temperature. However, the proton exchange between H_2 and D_2 molecules at high pressures and temperatures has hitherto received little attention. Shock compression experiment is a powerful technique for exploring the matter under extreme conditions. Chen *et al.* [32] carried out shock experiments for the gaseous $H_2 + D_2$ mixture by using two-stage light-gas gun and the sample was shocked to 140 MPa. Then Gu *et al.* [13] used the same loading tool to launch multi-shock compression experiments and extended the EOS of this mixture to 36 GPa. These experimental EOS data provide an opportunity to evaluate the exchange-correlation (XC) functionals implemented in first-principles molecular dynamic simulations.

For the theoretical aspects, research on this isotopic mixture is scarce. Collins *et al.* [33] presented quantum molecular dynamics (QMD) simulations on the diffusion coefficients of hydrogen at 0.38–0.52 g/cm^3 and 2000–30 000 K, but the viscosities were neglected. Clérouin and Dufrêche [34]

*chenqf01@gmail.com
†xrchen@scu.edu.cn

have performed the simulations on ionic transport properties of deuterium at low-density regimes (equivalent H mass densities of 0.33–0.75 g/cm^3) and temperatures of 1–50 kK by QMD simulations. Unfortunately, their QMD simulations were performed for only 3000 steps due to the limitations of the calculation conditions at the time, which is too small to arrive at the converged values for diffusion coefficient and viscosity. Kress *et al.* [6] used QMD and orbital free molecular dynamics (OFMD) diffusion coefficient and viscosity of D-T mixtures at high-density regimes (equivalent hydrogen mass densities between 2 and 8 g/cm^3) and temperatures of 2–10 eV as a benchmark to validate and verify several analytical one component plasma (OCP) models. However, they ignored the low-density regimes where the equivalent H mass density is less than 1 g/cm^3. Furthermore, in previous works [2,6,34–36], a simple exponential fitting function was widely used to fit time correlation functions to obtain diffusion coefficient and viscosity, but it might lead to inaccurate results for strongly coupled systems suggested by Meyer *et al.* [37] and Danel *et al.* [38]. Recently, Meyer *et al.* [37] presented another multi-time scale fitting function which has been successfully applied to pure elements and mixtures. Here we use the time correlation function of the H-D mixture calculated by QMD as an example to revisit the applicability of these two fitting functions.

In this paper, our main purpose is to explore the proton exchange, ionic structures, and transport properties of H-D mixtures over a fairly wide ρ–T region. Special emphasis will be made on the proton exchange and the topology analysis of ionic structures for this mixture. Moreover, the QMD calculated diffusion coefficient and viscosity were utilized as a benchmark to evaluate some analytical OCP models which are useful for studying ICF experiments and modeling the interior structure and evolution of giant planets if they are confirmed to be valid. The paper is organized as follows. The theoretical method and computational details are given in Sec. II. The results and some discussion are presented in Sec. III. Finally, the conclusions can be found in Sec. IV.

II. COMPUTATIONAL DETAILS AND THEORETICAL METHODS

A. Simulation methods

Quantum molecular dynamics simulations are performed using CP2K/QUICKSTEP program [39]. In these calculations, the Born-Oppenheimer molecular dynamics is used for propagation of the classic nuclei. CP2K adopts the hybrid Gaussian and plane waves method, which allows for fast and accurate density functional theory (DFT) calculations for large systems. The Goedecker-Teter-Hutter (GTH) pseudopotentials [40] together with the double zeta valence plus polarization (DZVP) basis sets have been utilized. The plane wave cutoff energy is set to be 500 Ry while the cutoff energy of the Gaussian type basis set is 40 Ry. The self-consistent field (SCF) guess is propagated using the always-stable predictor-corrector, and the SCF convergence criterion is set to be 10^{-5} a.u. The electron exchange-correlation potential is modeled by the Perdew-Burke-Ernzerhof (PBE) functional [41] in the generalized-gradient approximation (GGA). As is well known, the density functional theory cannot accurately describe dispersion forces with the GGA functional, which limits its applications to van der Waals (vdW) systems at low densities [42]. Thus we considered here two schemes to encompass the vdW interactions. One of them is the semiempirical force field correction method named DFT-D2 [43], and the other is the nonlocal exchange-correlation function vdW-DF1 [44].

All simulations are employed on point sampling of the Brillouin zone. A cubic cell containing 128 H and 128 D atoms with periodic boundary condition is used, and the size of the cell is determined by the mass density. Initially, the hydrogen and deuterium molecules are randomly distributed in a cubic cell of length L (volume $V = L^3$). The simulations have been performed in the canonical ensemble and the temperature of ions is controlled by a Nos-Hoover thermostat [45]. The temperature effects on electrons are taken into account by using the Fermi-Dirac smearing. The system is assumed to be in a thermodynamic equilibrium by setting the ion (T_i) and electron (T_e) temperatures to be equal. The time step used in QMD simulations varies between 0.2 and 0.5 fs with respect to different temperatures. Dynamic simulations are performed for at least 1 ps temporal duration to reach thermal equilibrium, and the total simulation time amounts up to 3–8 ps. The properties of the H-D mixture we studied span low- and high-density ranges (0.1–5 g/cm^3) and wide temperature ranges (1000–50 000 K), which is selected to compare with the ρ–T range of experimental multi-shock compression results and to cover the outer mantle region of the gas giant planets up to the inner core region.

B. Calculation of the ionic transport coefficients

The self-diffusion coefficients can be obtained by either the mean-square displacement [46],

$$D_R = \frac{1}{6t}\left\langle \left|\mathbf{R}_i^\alpha(t) - \mathbf{R}_i^\alpha(0)\right|^2 \right\rangle, \tag{1}$$

or the velocity autocorrelation function (VACF) using the Green-Kubo formula [46],

$$D_V = \lim_{t\to\infty} D_V(t) = \lim_{t\to\infty} \frac{1}{3}\int_0^t dt' \left\langle \mathbf{v}_i^\alpha(t') \cdot \mathbf{v}_i^\alpha(0) \right\rangle, \tag{2}$$

where $\mathbf{R}_i^\alpha(t)$ is the position of the ith atom of species α at time t; $\mathbf{v}_i^\alpha(t)$ is the center-of-mass velocity of the ith particle at time t. The angled bracket denotes an ensemble average.

Similarly, we compute mutual-diffusion coefficients from the mutual-diffusion current autocorrelation function (MCACF),

$$D_{\alpha\beta} = \lim_{t\to\infty} D_{\alpha\beta}(t) = \lim_{t\to\infty} \frac{Q}{3Nx_\alpha x_\beta}\int_0^t dt' \langle \mathbf{c}(t') \cdot \mathbf{c}(0) \rangle, \tag{3}$$

where $\mathbf{c}(t)$ is the mutual-diffusion current, and it can be written as follows:

$$\mathbf{c}(t) = x_\beta \sum_{i=1}^{N_\alpha} v_i^\alpha - x_\alpha \sum_{j=1}^{N_\beta} v_j^\beta. \tag{4}$$

The quantity Q denotes the thermodynamic factor. Research with the Lennard-Jones and other potentials have shown that even for different constituents the value of Q departs from unity only about 10% and the Q factor can be equal to unity for components with same charges and concentrations [6], so

that for an equimolar HD ($Z_1 = Z_2 = 1$) mixture, we set $Q = 1$. N_α and x_α represent the particle number of species α and concentration, respectively, and $N = \sum_\alpha N_\alpha$.

The viscosity η can be determined by the autocorrelations function of off-diagonal components of stress tensor (STACF),

$$\eta = \lim_{t\to\infty} \eta(t) = \lim_{t\to\infty} \frac{V}{k_B T} \int_0^t \langle \delta_{ij}(t') \cdot \delta_{ij}(0) \rangle, \quad (5)$$

where the T and V are the temperature and volume, respectively, and k_B is the Boltzmann constant. $\delta_{ij}(t)$ represents the averaged result for five independent off-diagonal components of the stress tensor $\delta_{xy}, \delta_{yz}, \delta_{zx}, (\delta_{xx}\text{-}\delta_{yy})/2$, and $(\delta_{yy}\text{-}\delta_{zz})/2$. The stress tensor is a property of the entire system, including no additional average over N_α particles, so the viscosity is subjected to greater statistical imprecision when compared with diffusion coefficient, and thus longer trajectories are needed [47].

In order to shorten the simulation time and avoid the noise in the long-time behavior of the time correlation function, a single exponential model was widely utilized to fit the time correlation function [6,35]. However, the VACFs and STACFs of strongly correlated systems and mixtures may exhibit oscillatory features and even a negative correlated region [37,47]. Thus, in such a situation, the single exponential function is not capable of reproducing all features of time correlation functions. Recently, Meyer *et al.* [37,48] suggested a fitting form with multi-time scale function for VACFs,

$$\langle \mathbf{v}(t) \cdot \mathbf{v}(0) \rangle = a_0 e^{-t/\tau_0} + \sum_i^j a_i e^{-t/\tau_i} [\cos(\omega_i t) + \alpha_i \sin(\omega_i t)], \quad (6)$$

where parameters τ_0, τ, ω_i, a_0, a_i and α_i were determined by a least-squares fit. We used parameter j up to 1 for H and D. Several works [47–49] concentrating on binary or multi-component mixtures have confirmed the high efficiency of this fitting method. With the combination of Eq. (2) and Eq. (4), the diffusion constant is written as follows:

$$D_\alpha = a_0 \tau_0 + \sum_{i=1}^j a_i \tau_i \frac{1 + \alpha_i \tau_i \omega_i}{1 + \tau_i^2 \omega_i^2}. \quad (7)$$

For STACFs, we used the two-exponential function proposed by Guo *et al.* [50] which is given by

$$\langle \delta(t) \cdot \delta(0) \rangle = b_0 e^{-t/\tau_0} + b_1 e^{-t/\tau_1} \cos(\omega_1 t), \quad (8)$$

where b_0, b_1, τ_0, τ_1 and ω_1 are the fitting parameters. Inserting Eq. (8) into Eq. (5), one can obtain the following expression for the viscosity:

$$\eta(t) = A\tau_0 + \frac{B\tau_1}{1 + (\tau_1 \omega_1)^2}. \quad (9)$$

The statistical errors of diffusion and viscosity suggested by Meyer *et al.* [37] are written as

$$\varepsilon_D = \sqrt{\frac{2}{N_i T_{\text{traj}}} \left(c_0 \tau_0 + \sum_{i=1}^j c_i \tau_i \frac{1 + \alpha_i \tau_i \omega_i}{1 + \tau_i^2 \omega_i^2} \right)}; \quad (10)$$

$$\varepsilon_\eta = \sqrt{\frac{2}{T_{\text{traj}}} \left(d_0 \tau_0 + d_1 \frac{\tau_1}{1 + \omega_1^2 \tau_1^2} \right)}, \quad (11)$$

respectively, where $c_i = a_i / \sum_i a_i$ and $d_i = b_i / \sum_i b_i$, N_i is the number of particles of species i in the simulation, and T_{traj} is the total trajectory time of the simulation. As suggested by Meyer *et al.* [37], a sliding time window t_w should be introduced to skip steps on the order of correlation time aiming at eliminating systematic error due to the similarities between snapshots close to each other. We use $t_w = 20$ fs for diffusion and $t_w = 10$ fs for viscosity at the density of 1 g/cm^3, while for the higher density of 5 g/cm^3, we choose $t_w = 8$ fs for diffusion and $t_w = 5$ fs for viscosity. t_w satisfies the criteria $\tau < t_w \ll T_{\text{traj}}$. τ is the longest decay time.

III. RESULTS AND DISCUSSION

A. Convergence test

Convergence tests are the prerequisite for MD simulations. The convergence tests with respect to the cutoff energies, system size, and simulation steps are displayed in Fig. 1. The results shown in Fig. 1(a) reveal that two cutoff energies of 500 and 40 Ry for plane waves and Gaussian basis set, respectively, used in our simulations already converge energy within 10^{-6} hartree/atom. In MD simulations, the size effect of the system should not be neglected. Thus, three different system sizes with 64, 128, and 256 atoms in the supercell at 1 g/cm^3 are tested for H-D mixtures. It can be seen from Fig. 1(b) that the calculated pressures and internal energies change within 1% when changing the number of atoms, indicating that they are insensitive to the number of atoms we are testing. For the diffusion coefficients and viscosities, the results with 64 atoms deviate more than 10% from those with 256 atoms at high temperatures while the results with 128 and 256 atoms show good convergence in the whole temperature range, as shown in Fig. 1(c). Therefore, it is safe to use 256 atoms in MD simulations. Diffusions and viscosities require very long trajectories to arrive at convergent values, especially for the viscosities. Consequently, here we make a convergence test of total trajectory time steps (T_{traj}) for STACFs. One can clearly see from Fig. 1(d) that the normalized STACFs exhibit good convergence when the T_{traj} increases up to 30 000 and 40 000. According to the tests, 40 000 steps are sufficient to obtain converged results.

B. Equation of state

Recent shock compression data of deuterium with unprecedented precision along the principal Hugoniot was used to evaluate XC functionals at the molecular-to-atomic transition [16]. Quasi-isentropic shock-compression experiments on hydrogen or deuterium were also modeled based on QMD data [51,52]. In addition, multi-shock EOS with respect to Ar [53] and Ne [54] were used to verify and validate the appropriate XC functionals, which shows that QMD simulations can give multi-shock states with good accuracy from adiabatic framework if the XC functionals are accurate. This impel us to use our previous multi-shock EOS of the H-D mixture [13] as a benchmark to evaluate several XC functionals. In the multi-shock experiment, a planar strong shock wave is produced by the impact of a Ta flyer driven by a two-stage light-gas gun. Multiple shocks in the dense gas H-D mixture are generated by a shock reverberation technique. It is confined in a cell with a

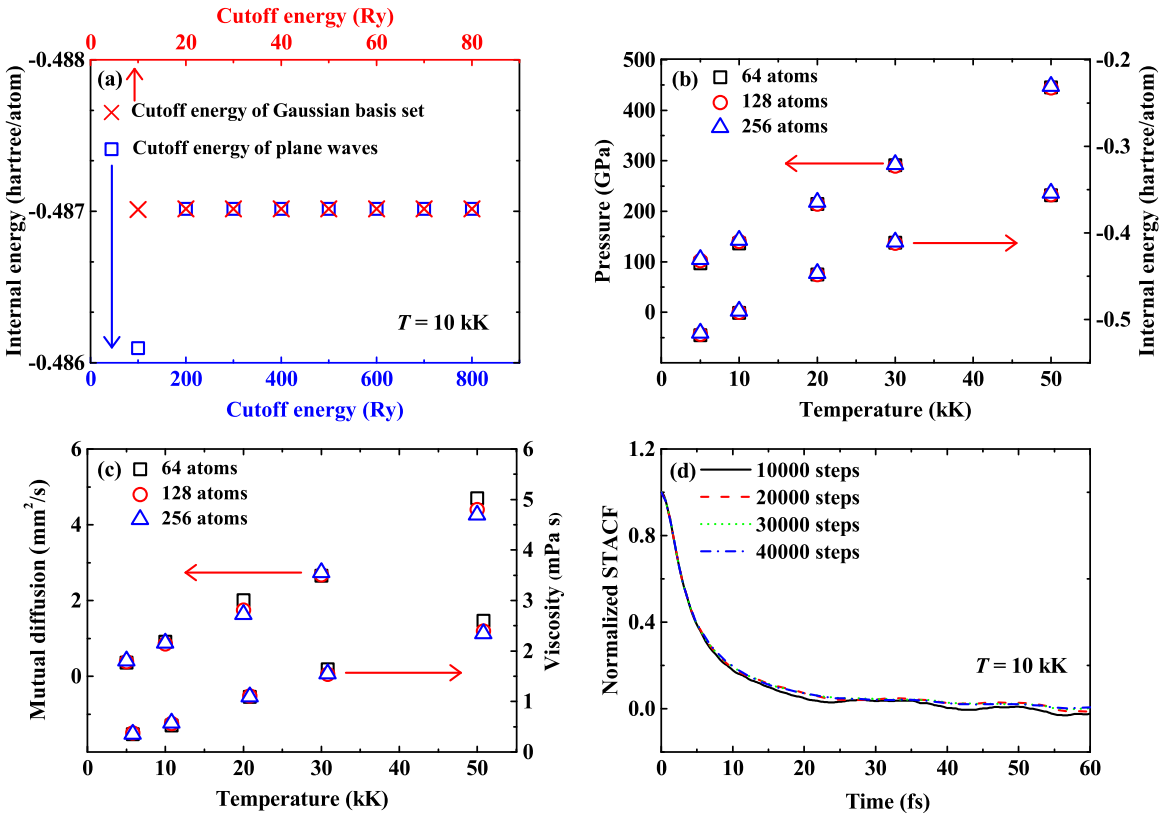

FIG. 1. Convergence tests on (a) the simulation cutoff energies, (b) particle numbers in the supercell for pressure and internal energy and (c) diffusion and viscosity, and (d) simulation steps at 1 g/cm^3.

304 steel baseplate at impact end and a LiF or saphire window at other end. As the shocks exit the baseplate and transmit into dense gas H-D mixture, the compressed mixture becomes hot and optically thick enough to enable recording the self-emission from the shock by using the multiple channel optical pyrometer [13,55]. Combination of experimental observables and impedance matching method, the multi-shock states can be determined. The initial sample was shocked into a pressure range of 236 GPa and a temperature range of 2300–5300 K after three-shock compressions.

The Hugoniot of H-D mixtures is calculated by the Rankine-Hugoniot relation,

$$E - E_0 = (P + P_0)(V_0 - V)/2, \tag{12}$$

where E_0, P_0, and V_0 are internal energy, pressure, and volume of initial state, respectively. And E, P, and V are the corresponding parameters of the final state. We calculated 100 temperature and density points for each XC functional in our simulations, covering a fairly wide range of densities (0.1–1 g/cm^3) and temperatures (1–10 kK). The Hugoniot is estimated from the intersections of the Hugoniot relation and the isothermal lines interpolated from the EOS. Challenges were encountered in modeling multi-shock EOS of the H-D mixture. QMD simulations are expensive in calculations, and the sizes of the system are usually limited to a few hundred atoms and the timescale is limited to a few picoseconds. Furthermore, the energy and pressure are difficult to arrive the converged values during simulating the initial state due to that the initial density of dense gas H-D mixture is as low as 0.04 g/cm^3. We used a more accurate basis set DZVP-MOLOPT-GTH to deal with this problem, which is suitable for calculations in the gas and in the condensed phase [56]. The experimental results of Gu *et al.* [13] and our calculated multi-shock EOS of H-D mixtures are shown in Fig. 2. One can see from Fig. 2 that the PBE and the vdW-DF1 give nearly the same results for the first shock state and agree well with the experimental data, while the DFT-D2 underestimates the first shock pressure. The values calculated by PBE and DFT-D2 are nearly the same for the second and the third shock states, and they agree well with the experimental second shock data but located outside the error bars of the third shock state. The third shock state estimated by vdW-DF1 agrees well with the experimental results. The MD simulations indicate that the vdW-DF1 functional can reasonably describe the experimental multi-shock EOS. Our conclusion is also supported by benchmarking QMC simulations by Clay *et al.* [57,58] and high precision measurements by Knudson and Desjarlais [16]. Their results show that vdW-DF1 is better suited for describing the properties for pure hydrogen as well as hydrogen-helium mixtures in many aspects [59]. Unfortunately, the multi-shock pressure and density are only up to 36 GPa and 0.55 g/cm^3, respectively, and the error bars of the third shock is too big due to the error propagation and accumulating. Thus future high-precision experimental data over a wide range of ρ–P are needed to further check the validation of these XC functionals.

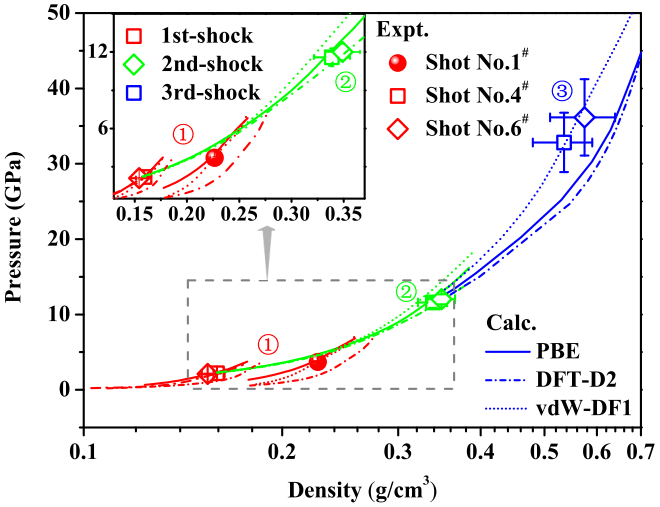

FIG. 2. The multi-shock EOS of Gu *et al.* [13] and our QMD results. The inset is an enlarged graph of the principal Hugoniot and the second-shock EOS.

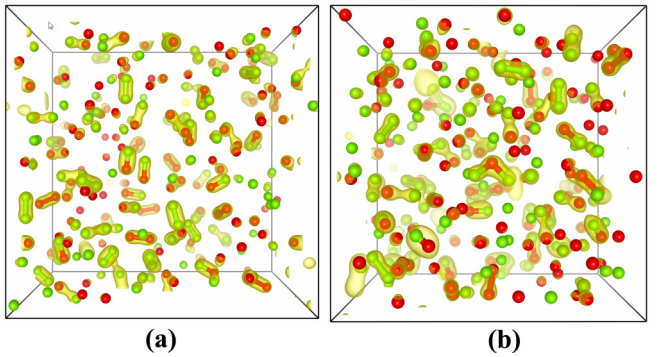

FIG. 4. Snapshots of the simulation box at (a) 4000 K and 0.5 g/cm^3 (b) 1500 K and 1 g/cm^3, visualized by the VESTA program [63] with depth cueing. Red balls represent hydrogen ions while green spheres are deuterium ions, and the electron density n_e of isosurfaces (yellow) is set to be 0.18 e/Å^3.

C. Structural dynamics

The dynamic structures of dense mixtures are essential to understand the dynamics of a gas-giant planets core [60]. The structures of warm dense H-D mixture have been rarely studied foretime. Our MD simulations cover a fairly wide $\rho-T$ range. Consequently, different dynamical behaviors are anticipated for this mixture. Here the ionic structures of H-D mixtures are first investigated by looking at the pair distribution functions (PDFs). The PDFs give the probability of ions around a given ion as a function of their distance, with respect to the uniform distribution of a noninteracting system [61]. The first peak of H-H, D-D, and H-D at around $r = 0.78$ Å corresponds to their bonds. From Fig. 3, we can see that at 4 kK for 0.5 g/cm^3 [Fig. 3(c)] and 1.5 kK for 1 g/cm^3 [Fig. 3(f)], a new peak in H-D PDFs locates at around $r = 0.78$ appears, indicating the formation of HD molecules, i.e., the proton exchange occurs. For further recognizing the formation of HD molecules, we examined the isosurfaces of the electron density for the above two thermodynamic states, as shown in Fig. 4. One can clearly observe from Figs. 4(a) and 4(b) that electronic densities are pronounced between H-D pairs, indicating a stable molecular

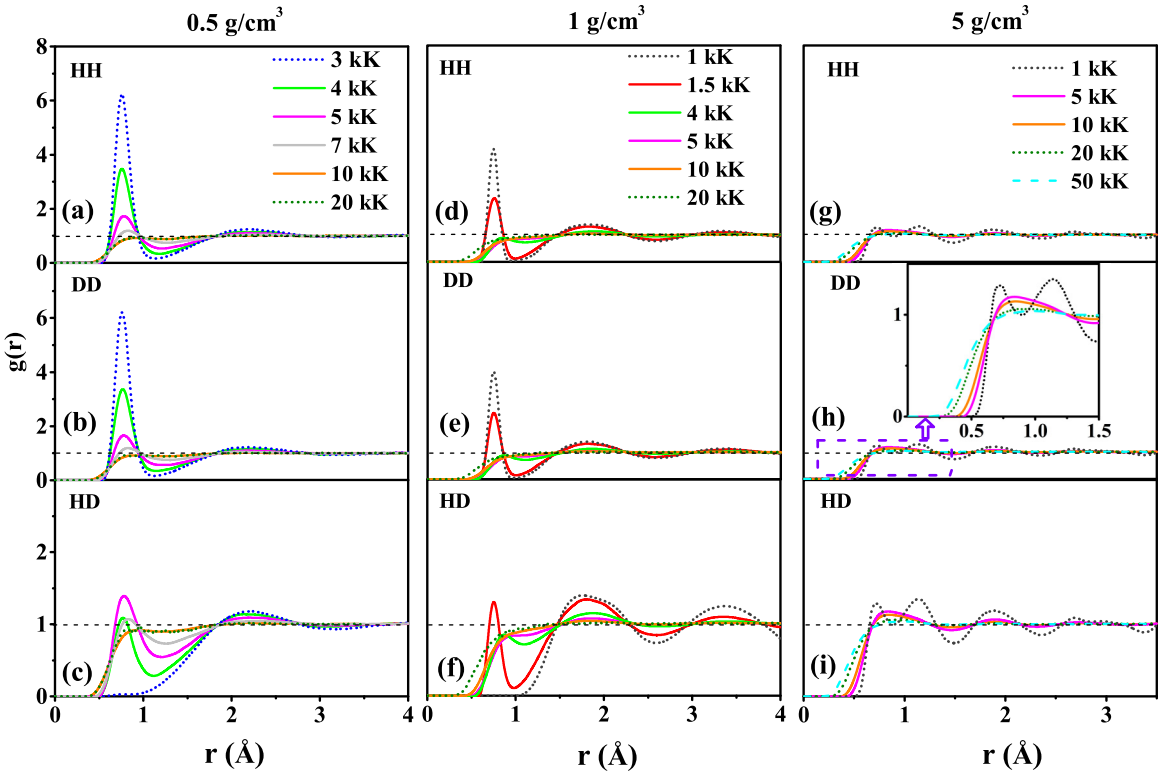

FIG. 3. The PDFs of H-H, D-D, and H-D at three densities and different temperatures. The insert in (h) is an enlarged picture of D-D PDFs.

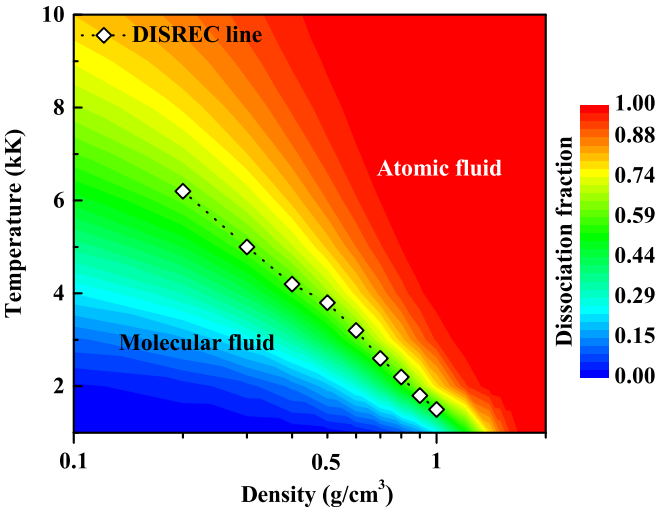

FIG. 5. The ρ–T contour of dissociation fraction and the boundary line of DISREC.

structure. The mechanism of the present proton exchange is very different from that observed in a previous diamond anvil cell experiment which was attributed to the quantum tunneling [29–31]. Over the $\rho-P$ region considered in this work, the nuclear De Broglie wavelength is much smaller than the internuclei distance so that the nuclear quantum effect can be ignored. According to the PDFs shown in Fig. 3, the appearance of HD molecules is accompanied by the rapid dissociation of H_2 and D_2 molecules. There is a probability that H and D atoms from the dissociated molecules recombine with each other. Thus, we prefer to believe that the formation of HD molecules can be interpreted as a process of dissociation followed by recombination (DISREC) [62]. The H-D mixture provides a unique opportunity to observe the proton exchange, which should be taken into account in future researches.

To reveal at what conditions the DISREC process would take place, we calculated the fraction of molecules in the system which can be derived from the coordination number as follows [25]:

$$K(r) = \frac{N-1}{V}\int_0^r 4\pi r'^2 g(r')dr', \tag{13}$$

where $g(r)$ are the PDFs of H-H, D-D, and H-D. N and V represent the total number of ions and volume of the supercell used in MD simulations, respectively. The r cut is set to be 0.748 Å. The DISREC can be considered to occur if the fraction of HD molecule is greater than or equal to 1%. The fraction of molecule was calculated along numerous isotherms. A diagram of dissociation degree together with a boundary line representing the appearance of DISREC process was constructed in Fig. 5 which shows that the DISREC process takes place when H_2 and D_2 molecules are almost 50% dissociated.

The PDFs at higher density of 5 g/cm^3 are shown in the right panel of Fig. 3. At $T = 1$ kK, PDFs of H-H, D-D, and H-D all show small peaks in a short range, which indicates a liquid behavior. For the higher temperatures ($T > 5$ kK), in the liquid region, only their first peaks are evident. Although their first peaks decease and broaden with the increase of temperatures, they remain up to 20 kK, as we can see from the insert graph of Fig. 3(h), which indicates the existence of the short-range ordered structures in the system.

The PDFs only qualitatively show the information of ionic structures, but they are unable to capture the specific information of the local structures in the system. To give details of ionic structures during the MD simulations, we used a categorizing method [64] for ionic structures. This method first finds the nearest atoms within a specific distance for each atom and then classifies these local structures into single, chain, circle, and cluster by counting the number of nearest atom. The specific distance between two atoms is the sum of the two effective bonding radii. The effective bonding radius of H can be determined by using the effective coordination number (ECN) model [65],

$$\mathrm{ECN} = \frac{1}{N}\sum_{i=1}^{N}\mathrm{ECN}_i = \frac{1}{N}\sum_{i=1}^{N}\sum_{j\neq i}\exp\left[1-\left(\frac{d_{ij}}{d_{\mathrm{av}}^i}\right)^6\right], \tag{14}$$

$$d_{\mathrm{av}}^i = \frac{\sum_j d_{ij}\exp\left[1-\left(\frac{d_{ij}}{d_{\mathrm{av}}^i}\right)^6\right]}{\sum_j \exp\left[1-\left(\frac{d_{ij}}{d_{\mathrm{av}}^i}\right)^6\right]}, \tag{15}$$

$$d_{\mathrm{av}} = \frac{1}{N}\sum_{i=1}^{N} d_{\mathrm{av}}^i, \tag{16}$$

where i, j are the indices of H atoms and d_{ij} is the distance between the ith and jth atoms. $d_{\mathrm{av}}/2$ is the effective bonding radius of H. By using this model, the ionic structure of warm dense iron [60], hydrogen [66], and silane [67] were successfully investigated. The calculated values of ECN and effective bonding diameter d_{av} of H atoms are shown in Fig. 6, from which we can see that the ECN and d_{av} at densities of 0.5 g/cm^3 and 1 g/cm^3 both have a rapid increase over the temperature range of 3–7 kK and 1–3 kK, respectively. Molecular dissociation induced by temperature is responsible for this. For the higher density of 5 g/cm^3, they both decrease gently with increasing temperature, indicating a continuous molecular-to-atomic transition.

The ECN model mentioned above can provide a quantitative description of the dynamic ionic structures of H-D mixtures during QMD simulations. The percentages of various local structures at two densities and different temperature are displayed in Fig. 7. The error of present method mainly comes from the statistical error of the effective bonding diameter d_{av}, and the error bars of d_{av} are supplied in Fig. 6. According to the error of d_{av}, we estimated that the fractions of single, chain, circle, and cluster structure are generally accurate within 1%, 2–3%, 5–7%, and 15–21%, respectively, depending on the density and temperature. For the density of 1 g/cm^3, the chain structure with two atoms (i.e., molecules) occupies 81% at 1 kK. For temperatures beyond 10 kK, molecules are almost completely dissociated, so the single structure takes up the largest proportions. For the higher density of 5 g/cm^3, the cluster structure is dominant, and it takes up to 74% at the temperature of 1 kK. With the increase of temperature, however, percentages of cluster structure decreases. It decomposes into circle, chain, and single structure. The

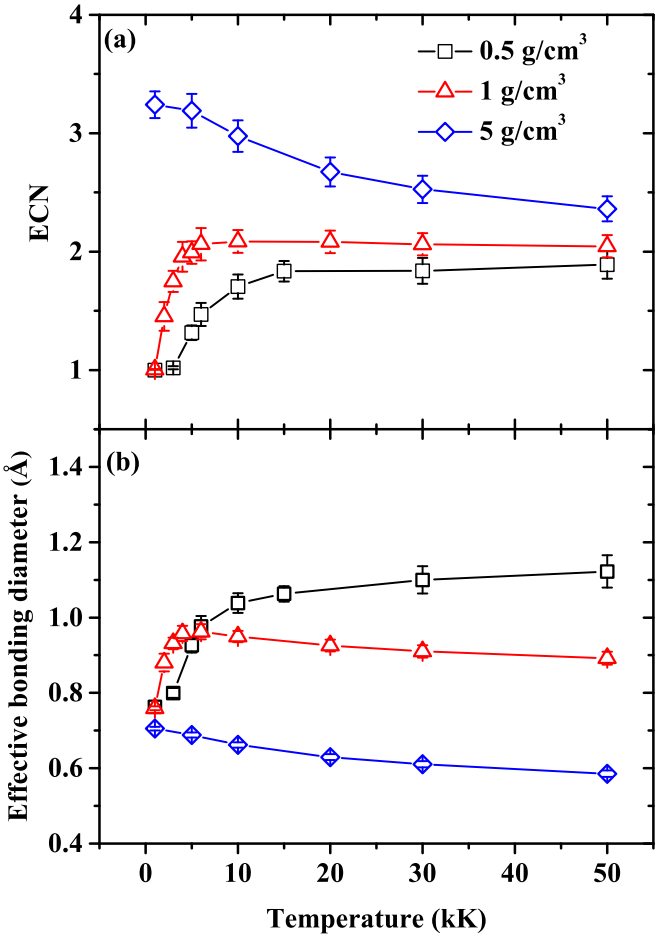

FIG. 6. The averaged values of ECN and effective bonding diameter d_{av} at three densities and different temperatures.

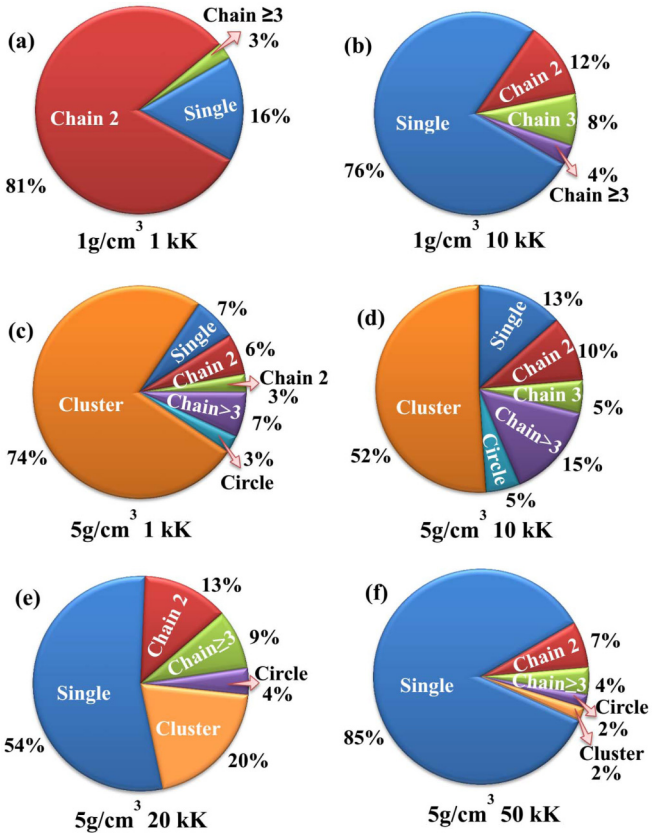

FIG. 7. Fractions of different dynamic structures at 1 and 5 g/cm^3 and different temperatures. Single, Chain 2, and Chain 3 represent the structures with single-atom, two-atom, and three-atom, respectively. Circle represents the circle structure with every atom in the structure owns only two nearest atoms in a circle. Cluster represents a complex structure whose central atom has more than three nearest atoms.

fraction of the cluster structure decreases to 52%, while the percentages of chain and circle structures increase up to 35% at $T = 10$ kK. These local structures are responsible for the short-range ordered nature shown in PDFs at 5 g/cm^3. For $T > 20$ kK, the total percentages of the cluster, the circle, and the chain structures are further decreased, and the system is predominantly composed of the single structure. Therefore, the first peaks of PDFs at 5 g/cm^3 disappeared at temperatures beyond 20 kK. It should be noted that even though these species shown in Figs. 5 and 7 may occupy fairly large fractions, they are transient bound states with short lifetime due to that there is a continuous formation and destruction of these structures, which is a typical characteristic of WDM.

The time correlation function is of great interest in computer simulations due to its clear picture of dynamics in a fluid system. In order to explore the influence of the different ionic structures on the dynamical behaviors during the QMD simulations, normalized VACFs of H and D at different pressures and temperatures are shown in Fig. 8. For the density of 1 g/cm^3, the negative correlation region and oscillatory features are evident on the normalized VACFs of H and D at 1 kK, as displayed in Fig. 8(a). The diatomic molecules are dominant under this condition in light of the dissociation diagram, so the oscillatory feature on VACFs is an embodiment of bonding effect [48]. At the temperatures beyond 5 kK, the dominant component is the single structure, so the normalized VACFs decay in the form of a single exponential function. For the higher density of 5 g/cm^3, complex cluster structure takes up large proportion at 1 kK in terms of the ECN model, which is responsible for the oscillatory and negative correlation region on the normalized VACFs. This is a manifestation of cage effect [68]. With the increase of temperature, the percentage of cluster structure decreases, thus the negative correlation region vanishes on the normalized VACFs, but the oscillatory feature is still distinguishable. At higher temperature ($T > 20$ kK), the single structure is dominant, so the normalized VACFs attenuate monotonously as a function of time.

D. Ionic transport coefficients

We took QMD calculated VACFs and MCACFs at 10 kK and two densities as an example to evaluate the two fitting forms: a multi-time scale function [i.e., Eq. (6) with $i = 1$)] and a single exponential formula [i.e., the first term of Eq. (6)]. The VACFs, MCACFs, and fitting results are shown in Fig. 9, together with diffusion coefficients D_V and D_{exp} derived by the two different fitting forms. At 1 g/cm^3, the two fitting forms both work very well with the difference between D_V and D_{exp} less than 4%. For the higher density of 5 g/cm^3, VACFs and MCACFs both exhibit oscillatory features, so the single

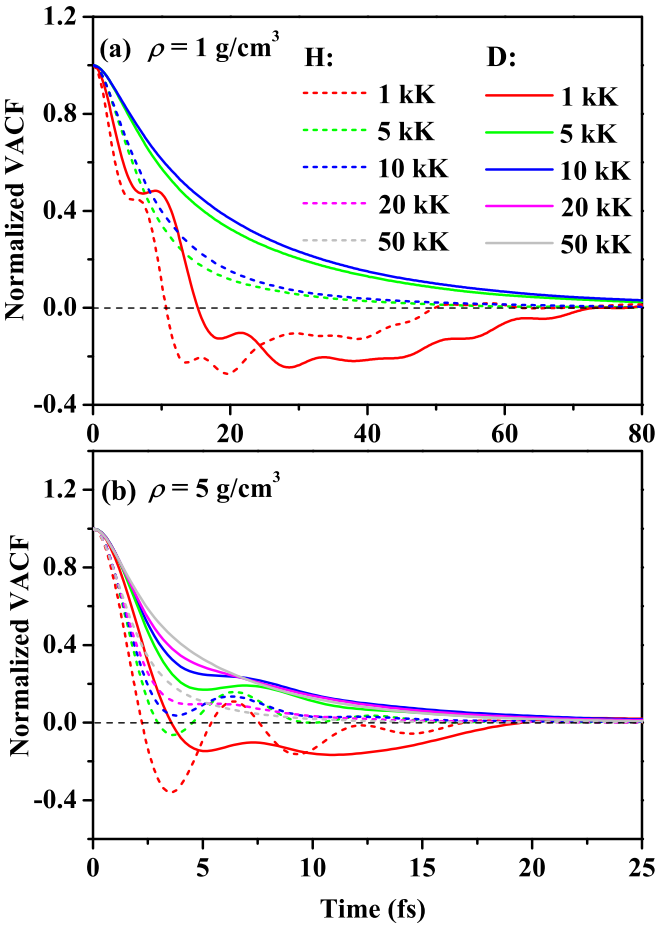

FIG. 8. The normalized VACFs of H and D at two representative densities and different temperatures.

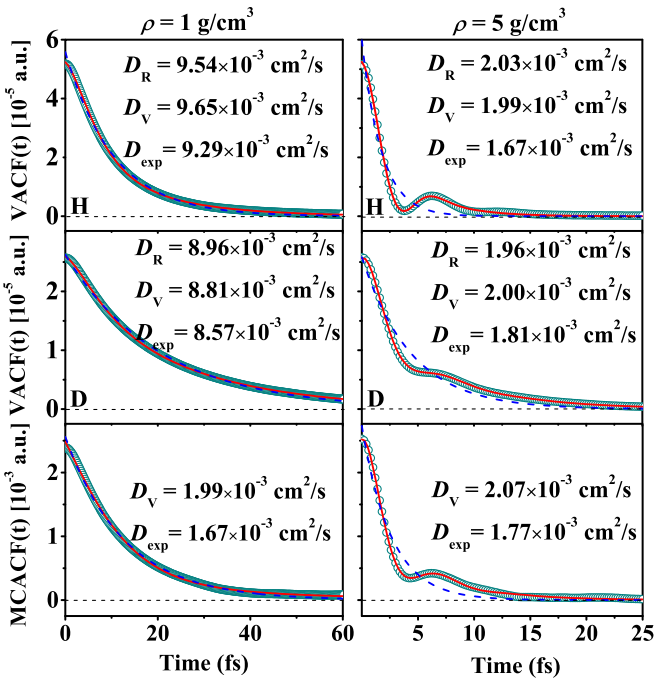

FIG. 9. VACFs and MCACFs of the H-D mixture at 1 g/cm^3 (left panel) and 5 g/cm^3 (right panel) and all at $T = 10$ kK. The present QMD data (dark cyan circles) are compared with the fitting results by a multi-time scale function (red solid line) and a single exponential fit (blue dashed line). D_R represents the self-diffusion coefficients obtained by Eq. (1), while the values of D_V and D_{exp} are extracted from the fitting of VACFs or MCACFs using Eq. (6) and the first term of Eq. (6), respectively. The VACFs and MCACFs are in atomic units.

exponential formulas cannot reproduce the VACFs well. The deviation between D_{exp} and D_V is larger than 10% for 5 g/cm^3. In addition, we computed the self-diffusion coefficient D_R by another way: the mean-square displacement, i.e., Eq. (1). Their values are given in Fig. 9. The deviation between D_V and D_R is within 2%, which confirms the convergence of our simulations.

Since the mutual-diffusion coefficient needs longer T_{traj} to arrive at converged value than the self-diffusion coefficient, we tested whether the Darken relation, i.e.,

$$D_{\alpha\beta} = X_\beta D_\alpha + X_\alpha D_\beta, \tag{17}$$

can be useful for calculating mutual-diffusion coefficients. As shown in Fig. 10, unlike the poor approximation of the Darken relation for H-He [47] and D-Ar mixtures [69], the Darken relation works very well for the equimolar mixtures of H-D at the considered temperatures and pressures. This is consistent with the results presented by Kress *et al.* [6]. They also suggested that the Darken relation is a good approximation for D-T mixtures.

Little attention has been paid to the influence of van der Waals interaction on the diffusion coefficient and viscosity. To this end, we make a comparison of transport coefficients calculated by PBE and vdW-DF1 functionals at the considered temperatures and densities in Figs. 11 and 12. The diffusion coefficient and viscosity obtained by the two different XC functionals generally agree with each other. The great difference between the vdW-DF1 results and the PBE data are seen at the highest temperature but within the margin of error.

Accurate knowledge of transport properties including diffusion coefficients and viscosities of materials are prerequisites

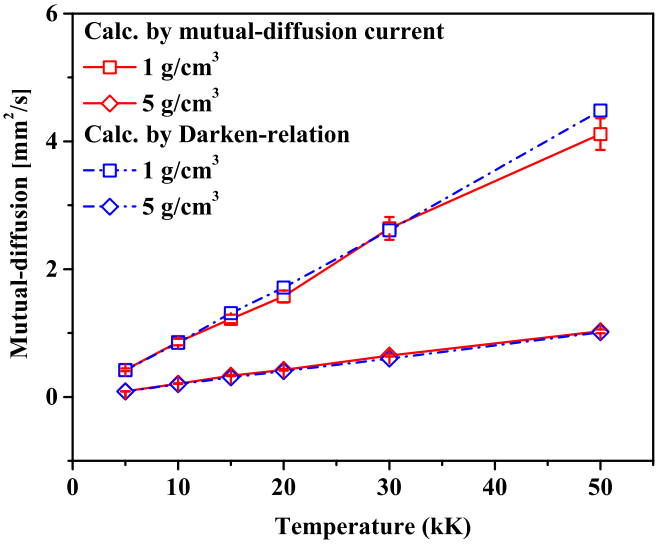

FIG. 10. Mutual diffusion coefficients at densities of 1 and 5 g/cm^3 and different temperatures.

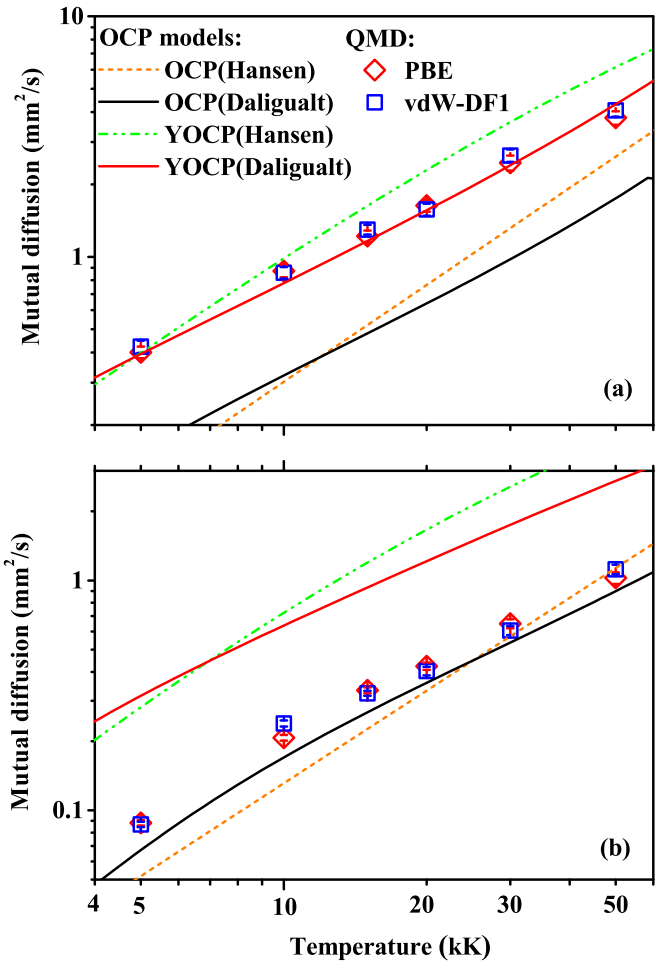

FIG. 11. Mutual-diffusion coefficients as a function of temperatures at densities of 1 g/cm^3 (top panel) and 5 g/cm^3 (bottom panel). Open red diamonds and open blue squares represent the results with PBE and vdW-DF1, respectively. Orange short-dashed and black solid curves are the OCP calculations of Hanson *et al.* [70] and Daligault [68], respectively. Green dash-dot-dotted and the red solid curves are the YOCP results based on the OCP models of Hanson *et al.* [70] and Daligault [68], respectively.

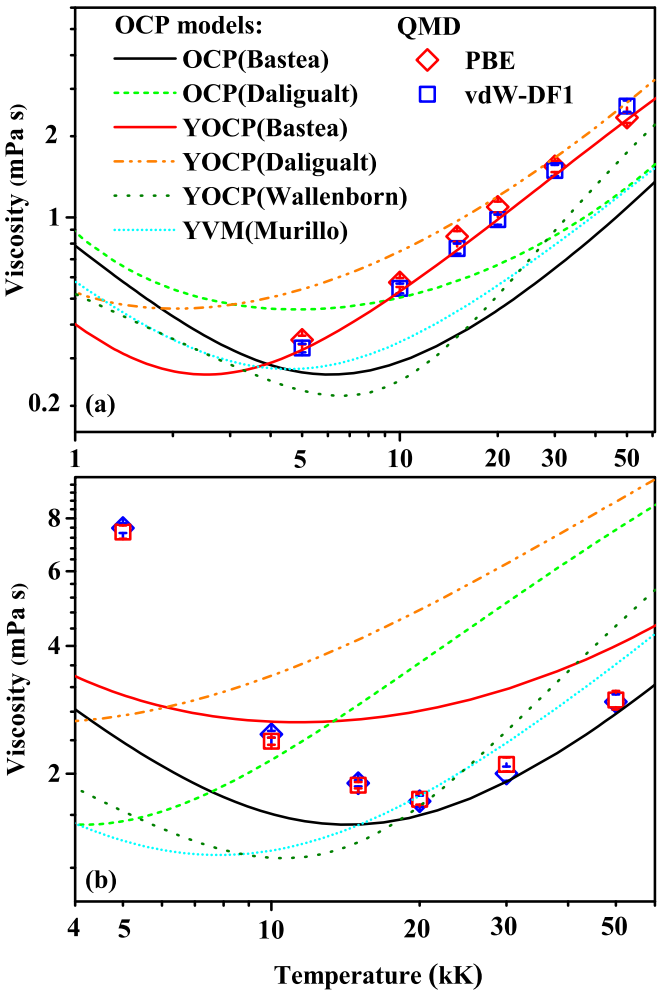

FIG. 12. Viscosities as a function of temperatures at densities of (a) 1 g/cm^3 and (b) 5 g/cm^3. Open red diamonds and open blue squares represent the results with PBE and vdW-DF1, respectively. Black solid and green short-short-dashed curves are the OCP calculations of Bastea [75] and Daligault [68], respectively. Red solid, the orange dash-dot-dotted, and the olive dotted curves are the YOCP results based on the OCP models of Bastea [75], Daligault [68], and Wallenborn [78], respectively. The cyan short-dotted curve is the YVM calculation of Murillo.

for radiation-hydrodynamics simulations, which is indispensable for designing and understanding ICF experiments [7]. Although QMD is a powerful method to estimate the ionic transport properties, it is not good for yielding large amounts of data at a small cost. An alternative method is to derive transport coefficients from the analytical OCP models, but they can only be used after validation. The Coulomb OCP model represents a system of interacting ions, with the bare Coulomb potential in a neutralizing uniform background of electrons [70]. The OCP models only depend on one dimensionless ionic coupled parameter,

$$\Gamma = \frac{Z^2 e^2}{a k_B T}, \tag{18}$$

where Z is the ion charge. In a binary system [71], $z^2 = \langle Z^* \rangle^{1/3} \langle (Z^*)^{5/3} \rangle$, $\langle Z^* \rangle = \sum_\alpha x_\alpha Z^*_\alpha$, x_α and Z^*_α represent concentrations and average ionization value for species α, respectively. In addition,

$$a = \left(\frac{3}{4\pi n} \right)^{1/3} \tag{19}$$

is the Wigner-Seitz radius of the ions for ion number density n.

In OCP models, the diffusion coefficient and viscosity are often expressed as the dimensionless quantities D^* and η^*, respectively,

$$D^* = \frac{D}{\omega_p a^2}; \quad \eta^* = \frac{\eta}{n M \omega_p a^2}, \tag{20}$$

and the plasma frequency ω_p for ions of mass M is given by

$$\omega_p = (4\pi n/M)^{1/2} Ze, \tag{21}$$

where M is the average mass of hydrogen and deuterium for the equimolar H-D mixture. Several analytical forms of the OCP model have been proposed. Hansen *et al.* [70] generated a fit of $D^* = 2.95\Gamma^{-1.34}$ using a memory function analysis of the VACFs for the classical OCP. Daligault [68] presented a rational function for D^* and η^* according to MD results for OCP. Murillo [72] suggested a Yukawa one-component plasmas (YOCP) model, in which the polarization of electrons close to each ion is accounted for through a Yukawa potential. Their suggested modified ionic coupled parameter Γ is given as follows:

$$\Gamma_{\mathrm{mod}} = A(\kappa) + B(\kappa)\Gamma + C(\kappa)\Gamma^2, \tag{22}$$

$$A(\kappa) = \frac{0.46\kappa^4}{1 + 0.44\kappa^4}, \tag{23}$$

$$B(k) = 1.01e^{-0.92\kappa}, \tag{24}$$

$$C(\kappa) = -3.7\times10^{-5} + 9.0\times10^{-4}\kappa - 2.9\times10^{-4}\kappa^2, \tag{25}$$

where κ is an inverse screening length. The parameter κ reduces into the inverse Thomas-Fermi screening length λ_{TF} in the case of degenerate electron fluids [73], and λ_{TF} is given by

$$\lambda_{\mathrm{TF}} = \left(\frac{\pi}{12Z}\right)^{1/3}\sqrt{r_s}, \tag{26}$$

where $r_s = a/a_0$ is the reduced Wigner-Seitz radius. $a_0 \equiv \hbar^2/m_e e^2$ is the Bohr radius.

In this work, average ionization values of Z^* at different temperatures and densities are computed using average atom model [74]. This model obtains the atomic average ionization degree through a relativistic Hatree-Fock-Slater SCF scheme. Since the value of Z^* is almost constant at a specific density and temperatures of 5–50 kK, we only give the values for different densities. The calculated values of Z^* are 0.65 and 0.95 for $\rho = 1$ g/cm^3 and $\rho = 5$ g/cm^3, respectively. And their corresponding values of κ are 1.07 and 1.59.

It is worth noting that these OCP models are appropriate only for atomic fluids. For the density of 1 g/cm^3, molecules in the system are fully dissociated when $T > 5$ kK in terms of the aforementioned dissociation diagram. Thus, we can see from Fig. 11(a) that YOCP (Daligault) calculations agree well with QMD results at temperatures beyond 5 kK, indicating that the system behaves like a kind of strongly screened plasmas under this specific condition. Clérouin and Dufrêche [34] have also suggested that YOCP calculations are in good agreement with QMD results for deuterium at the low density. Although both OCP models underestimate the diffusion coefficients, Daligault's OCP result is gradually approaching the QMD data with increasing temperatures. We can infer that the Daligault's OCP model will be consistent with QMD results when the temperature is above 50 kK, where the screening effect can be ignored. For another higher density, 5 g/cm^3 and $T < 20$ kK, the H-D mixture is mainly composed of high-order structures, such as clusters, circles, and long chains, as illustrated in Figs. 7(c) and 7(d). The system cannot be seen as a kind of well-defined atomic fluid under this condition, so the OCP and YOCP results both disagree with QMD data. When $T \geqslant 20$ kK, the single structure occupies the largest proportion, so the Daligault's and Hanson's OCP calculations agree with QMD results. This indicates that the system behaves like a kind of dense plasma at this thermodynamic condition. It can be seen from Fig. 11(b) that YOCP calculations significantly disagree with the QMD results. Kress *et al.* [6] also suggested the worse performance of the YOCP calculation for D-T mixtures at the high densities. We consider that the screening effect by electrons in the plasmas is very weak at the density of 5 g/cm^3, and it is not desirable to artificially insert a screening parameter in the bare coulomb potential.

For viscosity, Bastea [75] carried out classical MD simulations of the OCP and obtained the following fitting form:

$$\eta^* = A\Gamma^{-2} + B\Gamma^{-s} + C\Gamma, \tag{27}$$

where $s = 0.878$, $A = 0.482$, $B = 0.629$, and $C = 0.00188$. Murillo [76] generated a Yukawa viscosity model (YVM) according to the MD results of Saigo and Hamaguchi [77]. In this model, viscosity η is given by

$$\frac{\eta}{\eta_0} = 0.0051\frac{\Gamma_m}{\Gamma} + 0.374\frac{\Gamma}{\Gamma_m} + 0.022, \tag{28}$$

where η_0 is the characteristic viscosity,

$$\eta_0 = \omega_p e^{-0.2\kappa^{1.62}} Mna^2, \tag{29}$$

and Γ_m is the melt boundary,

$$\Gamma_m = 171.8 + 82.8(e^{0.565k^{1.38}} - 1). \tag{30}$$

It can be seen from Fig. 12 that similar to the case of diffusion coefficients, the YOCP (Bastea) calculations are consistent with the QMD results at 1 g/cm^3. For the higher density of 5 g/cm^3, the OCP calculations of Bastea are consistent with QMD results when $T > 20$ kK. Kress *et al.* [6] also proposed that the Basteas OCP agrees better with QMD results at $T > 2$ eV and high densities, since the degeneracy of electrons is higher. Interestingly, for the density of 1 g/cm^3, the viscosity calculated by the YOCP (Bastea) model shows a shallow minimum at $T = 2.5$ kK. The QMD results should also display the shallow minimum on viscosity, but the temperature region where the shallow minimum emerges is out of our QMD studied range. Clérouin and Dufrêche [34] also observed this shallow minimum for deuterium at low densities and believed that this effect is an indication of crossover between an atomic behavior and a screened plasma behavior. For the density of 5 g/cm^3, according to the ECN model mentioned above, the system can only be regarded as a dense plasma when $T > 20$ kK, so the crossover shifts to the higher temperature range ($T \sim 20$ kK). Why does such a crossover only appear on the viscosity rather than on the diffusion constant? Viscosity arises from the transport of momentum, which is governed not only by the bodily movement of particles but also by the action of interparticle forces at a distance [68]. The two mechanisms compete with each other at different temperatures. As a consequence, a crossover on viscosity may emerge when the two mechanisms contribute to similar magnitude.

We compared our results with those available for pure H and H-He mixtures under the similar thermodynamic conditions to investigate how the ionic transport properties of the liquids vary when D or He is mixed into H, as shown in Fig. 13.

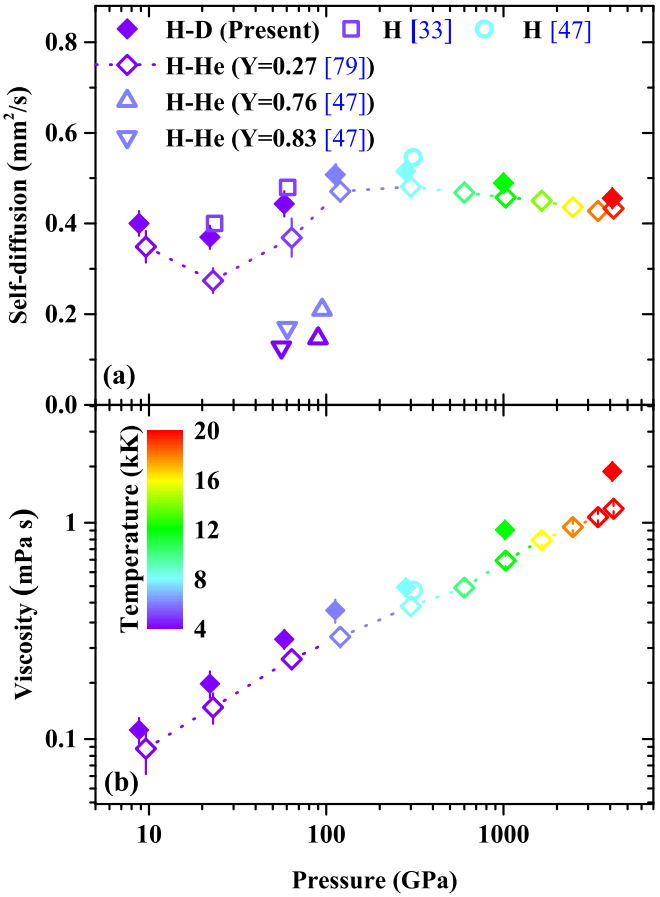

FIG. 13. The self-diffusion coefficients of H (a) and viscosities (b) in H-D mixtures, which are compared with those in pure hydrogen [33,47] and H-He mixtures with different He mass concentrations (Y) [47,79]. Colors indicate temperature (inset scale).

It can be seen from Fig. 13 that diffusion coefficients and viscosities for pure H are close to those for H-D mixtures, indicating that the inclusion of D has a little influence on ionic transport properties. At $T < 5000$ K and $P < 100$ GPa, diffusion coefficients of H in H-He mixtures with different He concentrations are obviously smaller than those in H-D mixtures. This is because the molecule H_2 bonds in H-He mixtures are shortened as well as strengthened compared to pure H as reported in Ref. [80], which will leads to smaller diffusions. At higher temperature and pressure, where the hydrogen molecules are dissociated, He has little influence on diffusions of H. Thus, diffusions of H in H-He ($Y = 0.27$) and H-D mixtures gradually merge together, as shown in Fig. 13(a). We can see from Fig. 13(b) that viscosities of H-He mixtures are smaller than those of H-D mixtures in the whole thermodynamic region because the viscosities of the liquids will decrease with the inclusion of He [47].

IV. CONCLUSION

The equation of state, proton exchange, dynamic structures, diffusion coefficients, and viscosities of H-D mixtures in the WDM regime have been elaborately studied using QMD simulations. The multi-shock EOS validates that the XC functional vdW-DF1 works best at the considered densities and temperatures. A dissociation diagram of H-D mixtures over a fairly wide $\rho-T$ range was obtained, which denotes a rough boundary between molecular and atomic fluids. The proton exchange between H_2 and D_2 molecules occurs at which the molecules in the H-D mixtures are almost half dissociated, which can be interpreted as a process of dissociation followed by recombination. The local structures were quantitatively analyzed by the ECN model. High-order structures like chain, circle, and cluster appear with the increase of density, but they decompose into single structure with increasing temperature. These local structures are responsible for different dynamic behaviors on VACFs. The negative correlation region and oscillatory features on VACFs at the low density of 1 g/cm^3 and the higher density of 5 g/cm^3 are due to the bonding effect and the cage effect, respectively. QMD calculated transport coefficients are used as a benchmark to check the validation of the analytical Coulomb and Yukawa OCP models. At 1 g/cm^3 and 5–50 kK, the Yukawa OCP calculations agree well with QMD results. Consequently, the system behaves like a kind of strongly screened plasma under this thermodynamic condition. For the higher density of 5 g/cm^3, the Coulomb OCP calculations are consistent with QMD data when $T > 20$ kK. Therefore, the system can be regarded as a kind of dense plasma only at temperatures beyond 20 kK.

ACKNOWLEDGMENTS

This work was supported by the Science Challenge Project (Grant No. TZ2016001), the National Natural Science Foundation of China (Grant No. 11674292), the Science and Technology Development Foundation of China Academy of Engineering Physics (Grants No. 2013A0101001 and No. 2015B0102001), the President Foundation of China Academy of Engineering Physics (201501032), the Foundation of Laboratory of Shock Wave and Detonation Physics of China Academy of Engineering Physics (Grant No. 9140C670103150C67289), and the National Postdoctoral Program for Innovative Talents (Grant No. BX201700215).

[1] J. E. Bailey, M. D. Knudson, A. L. Carlson, G. S. Dunham, M. P. Desjarlais, D. L. Hanson, and J. R. Asay, Phys. Rev. B **78**, 144107 (2008).
[2] Z.-G. Li, Y. Cheng, Q.-F. Chen, and X.-R. Chen, Phys. Plasmas **23**, 052701 (2016).
[3] F. Lambert, V. Recoules, A. Decoster, J. Clérouin, and M. Desjarlais, Phys. Plasmas **18**, 056306 (2011).
[4] T. Guillot, Science **286**, 72 (1999).
[5] J. J. Lissauer, Nature **419**, 355 (2002).
[6] J. D. Kress, J. S. Cohen, D. A. Horner, F. Lambert, and L. A. Collins, Phys. Rev. E **82**, 036404 (2010).
[7] S. X. Hu, V. N. Goncharov, T. R. Boehly, R. L. McCrory, S. Skupsky, L. A. Collins, J. D. Kress, and B. Militzer, Phys. Plasmas **22**, 056304 (2015).
[8] B. Xu and S. X. Hu, Phys. Rev. E **84**, 016408 (2011).
[9] B. Militzer, Phys. Rev. B **87**, 014202 (2013).

[10] D. C. Swift, J. H. Eggert, D. G. Hicks, S. Hamel, K. Caspersen, E. Schwegler, G. W. Collins, N. Nettelmann, and G. J. Ackland, Astrophys. J. **744**, 59 (2012).

[11] J. J. Fortney and N. Nettelmann, Space Sci. Rev. **152**, 423 (2009).

[12] W. J. Nellis, A. C. Mitchell, M. Van Thiel, G. J. Devine, R. J. Trainor, and N. Brown, J. Chem. Phys. **79**, 1480 (1983).

[13] Y. J. Gu, Q. F. Chen, J. Zheng, L. C. Cai, O. H. Jia, Z. Y. Chen, and F. Q. Jing, J. Appl. Phys. **111**, 013513 (2012).

[14] M. D. Knudson, D. L. Hanson, J. E. Bailey, C. A. Hall, J. R. Asay, and C. Deeney, Phys. Rev. B **69**, 144209 (2004).

[15] M. D. Knudson, M. P. Desjarlais, A. Becker, R. W. Lemke, K. R. Cochrane, M. E. Savage, D. E. Bliss, T. R. Mattsson, and R. Redmer, Science **348**, 1455 (2015).

[16] M. D. Knudson and M. P. Desjarlais, Phys. Rev. Lett. **118**, 035501 (2017).

[17] D. G. Hicks, T. R. Boehly, P. M. Celliers, J. H. Eggert, S. J. Moon, D. D. Meyerhofer, and G. W. Collins, Phys. Rev. B **79**, 014112 (2009).

[18] T. Sano, N. Ozaki, T. Sakaiya, K. Shigemori, M. Ikoma, T. Kimura, K. Miyanishi, T. Endo, A. Shiroshita, H. Takahashi, T. Jitsui, Y. Hori, Y. Hironaka, A. Iwamoto, T. Kadono, M. Nakai, T. Okuchi, K. Otani, K. Shimizu, T. Kondo, R. Kodama, and K. Mima, Phys. Rev. B **83**, 054117 (2011).

[19] P. Loubeyre, S. Brygoo, J. Eggert, P. M. Celliers, D. K. Spaulding, J. R. Rygg, T. R. Boehly, G. W. Collins, and R. Jeanloz, Phys. Rev. B **86**, 144115 (2012).

[20] G. V. Boriskov, A. I. Bykov, R. I. Il'kaev, V. D. Selemir, G. V. Simakov, R. F. Trunin, V. D. Urlin, A. N. Shuikin, and W. J. Nellis, Phys. Rev. B **71**, 092104 (2005).

[21] Q. F. Chen, L. C. Cai, Y. J. Gu, J. Zheng, and G. F. Ji, Phys. Lett. A **374**, 3875 (2010).

[22] M. Ross, Phys. Rev. B **58**, 669 (1998).

[23] G. Chabrier and A. Y. Potekhin, Phys. Rev. E **58**, 4941 (1998).

[24] B. Militzer and D. M. Ceperley, Phys. Rev. Lett. **85**, 1890 (2000).

[25] B. Holst, R. Redmer, and M. P. Desjarlais, Phys. Rev. B **77**, 184201 (2008).

[26] W. Lorenzen, B. Holst, and R. Redmer, Phys. Rev. Lett. **102**, 115701 (2009).

[27] F. Soubiran, S. Mazevet, C. Winisdoerffer, and G. Chabrier, Phys. Rev. B **87**, 165114 (2013).

[28] G. M. Borstad and C. S. Yoo, J. Chem. Phys. **135**, 174508 (2011).

[29] D. M. Brown and W. B. Daniels, Phys. Rev. A **45**, 6429 (1992).

[30] P. Loubeyre, R. LeToullec, and J. P. Pinceaux, Phys. Rev. B **45**, 12844 (1992).

[31] R. T. Howie, I. B. Magdau, A. F. Goncharov, G. J. Ackland, and E. Gregoryanz, Phys. Rev. Lett. **113**, 175501 (2014).

[32] Q. Chen, L. Cai, D. Chen, and F. Jing, Physica B **348**, 299 (2004).

[33] L. A. Collins, S. R. Bickham, J. D. Kress, S. Mazevet, T. J. Lenosky, N. J. Troullier, and W. Windl, Phys. Rev. B **63**, 184110 (2001).

[34] J. Clérouin and J. F. Dufrêche, Phys. Rev. E **64**, 066406 (2001).

[35] C. Wang, Y. Long, X. T. He, J. F. Wu, W. H. Ye, and P. Zhang, Phys. Rev. E **88**, 013106 (2013).

[36] D. A. Horner, F. Lambert, J. D. Kress, and L. A. Collins, Phys. Rev. B **80**, 024305 (2009).

[37] E. R. Meyer, J. D. Kress, L. A. Collins, and C. Ticknor, Phys. Rev. E **90**, 043101 (2014).

[38] J. F. Danel, L. Kazandjian, and G. Zerah, Phys. Rev. E **85**, 066701 (2012).

[39] J. VandeVondele, M. Krack, F. Mohamed, M. Parrinello, T. Chassaing, and J. Hutter, Comput. Phys. Commun. **167**, 103 (2005).

[40] S. Goedecker, M. Teter, and J. Hutter, Phys. Rev. B **54**, 1703 (1996).

[41] J. P. Perdew, K. Burke, and M. Ernzerhof, Phys. Rev. Lett. **80**, 891 (1998).

[42] T. Van Mourik and R. J. Gdanitz, J. Chem. Phys. **116**, 9620 (2002).

[43] S. Grimme, J. Chem. Phys. **124**, 034108 (2006).

[44] M. Dion, H. Rydberg, E. Schröder, D. C. Langreth, and B. I. Lundqvist, Phys. Rev. Lett. **92**, 246401 (2004).

[45] S. Nosé, J. Chem. Phys. **81**, 511 (1984).

[46] M. P. Allen and D. J. Tildesley, *Computer Simulation of Liquids* (Oxford University Press, Oxford, 2017).

[47] Z.-G. Li, W. Zhang, Z.-J. Fu, J.-Y. Dai, Q.-F. Chen, and X.-R. Chen, Phys. Plasmas **24**, 052903 (2017).

[48] E. R. Meyer, C. Ticknor, M. Bethkenhagen, S. Hamel, R. Redmer, J. D. Kress, and L. A. Collins, J. Chem. Phys. **143**, 164513 (2015).

[49] F. Soubiran, B. Militzer, K. P. Driver, and S. Zhang, Phys. Plasmas **24**, 041401 (2017).

[50] G.-J. Guo, Y.-G. Zhang, K. Refson, and Y.-J. Zhao, Mol. Phys. **100**, 2617 (2002).

[51] A. Becker, N. Nettelmann, B. Holst, and R. Redmer, Phys. Rev. B **88**, 045122 (2013).

[52] A. V. Chentsov and P. R. Levashov, Contrib. Plasma Phys. **52**, 33 (2012).

[53] H. Sun, D. Kang, J. Dai, W. Ma, L. Zhou, and J. Zeng, J. Chem. Phys. **144**, 124503 (2016).

[54] J. Tang, Y. J. Gu, Q. F. Chen, Z. G. Li, J. Zheng, C. J. Li, and J. T. Li, Phys. Rev. B **97**, 140101(R) (2018).

[55] Q. F. Chen, J. Zheng, Y. J. Gu, Y. L. Chen, L. C. Cai, and Z. J. Shen, J. Chem. Phys. **140**, 074202 (2014).

[56] J. VandeVondele and J. Hutter, J. Chem. Phys. **127**, 114105 (2007).

[57] R. C. Clay, J. Mcminis, J. M. McMahon, C. Pierleoni, D. M. Ceperley, and M. A. Morales, Phys. Rev. B **89**, 184106 (2014).

[58] R. C. Clay, M. Holzmann, D. M. Ceperley, and M. A. Morales, Phys. Rev. B **93**, 035121 (2016).

[59] M. Schöttler and R. Redmer, Phys. Rev. Lett. **120**, 115703 (2018).

[60] J. Dai, Y. Hou, D. Kang, H. Sun, J. Wu, and J. Yuan, New J. Phys. **15**, 045003 (2013).

[61] N. Desbiens, P. Arnault, and J. Clérouin, Phys. Plasmas **23**, 092120 (2016).

[62] R. P. Dias, O. Noked, and I. F. Silvera, Phys. Rev. Lett. **116**, 145501 (2016).

[63] K. Momma and F. Izumi, J. Appl. Cryst. **44**, 1272 (2011).

[64] J. Dai, Y. Hou, and J. Yuan, High Energy Density Phys. **7**, 84 (2011).

[65] M. J. Piotrowski, P. Piquini, and J. L. F. Da Silva, Phys. Rev. B **81**, 155446 (2010).

[66] D. Kang and J. Dai, J. Phys.: Condens. Matter **30**, 073002 (2018).

[67] H. Sun, D. Kang, J. Dai, J. Zeng, and J. Yuan, Phys. Rev. E **89**, 022128 (2014).

[68] J. Daligault, Phys. Rev. Lett. **96**, 065003 (2006).

[69] T. Haxhimali, R. E. Rudd, W. H. Cabot, and F. R. Graziani, Phys. Rev. E **90**, 023104 (2014).

[70] J. P. Hansen, I. R. McDonald, and E. L. Pollock, Phys. Rev. A **11**, 1025 (1975).
[71] J. P. Hansen, G. M. Torrie, and P. Vieillefosse, Phys. Rev. A **16**, 2153 (1977).
[72] M. S. Murillo, Phys. Rev. E **62**, 4115 (2000).
[73] J. Daligault, Phys. Rev. E **86**, 047401 (2012).
[74] X.-J. Meng and R.-L. Wang, Chinese J. Comp. Phys. **35**, 138 (2018).
[75] S. Bastea, Phys. Rev. E **71**, 056405 (2005).
[76] M. S. Murillo, High Energy Density Phys. **4**, 49 (2008).
[77] T. Saigo and S. Hamaguchi, Phys. Plasmas **9**, 1210 (2002).
[78] J. Wallenborn and M. Baus, Phys. Rev. A **18**, 1737 (1978).
[79] M. French, W. Lorenzen, M. Bethkenhagen, J. Wicht, and R. Redmer, Astrophys. J. Suppl. Ser. **202**, 5 (2012).
[80] J. Vorberger, I. Tamblyn, B. Militzer, and S. A. Bonev, Phys. Rev. B **75**, 024206 (2007).